ARTICLE

Hydrostatic pressure dependence in tensile and compressive behavior of an acrylonitrile–butadiene–styrene copolymer

Wilco M. H. Verbeeten[1] | **Miguel Sánchez-Soto[2]** | **Maria Lluisa Maspoch[2]**

[1]Structural Integrity Research Group, Universidad de Burgos, Burgos, Spain

[2]Centre Català del Plàstic (CCP), Departament de Ciència i Enginyeria de Materials, Universitat Politècnica de Catalunya, BARCELONATECH, Barcelona, Spain

Correspondence
Wilco M.H. Verbeeten, Structural Integrity Research Group, Universidad de Burgos, Burgos, Spain.
Email: wverbeeten@ubu.es

Abstract

The strain-rate dependence of a commercial grade ABS copolymer has been analyzed in both compression and tension. By measuring in two loading geometries, the hydrostatic pressure-dependence on the material's deformation behavior can be established. An alternative method to determine pressure-dependence, based on the difference in strain-rate dependence for various loading geometries, has been presented. It was shown to be an effective technique, both for thermorheologically simple materials such as ABS, as well as thermorheologically complex materials, for example, PMMA. A yield criterion, based on an Eyring-type pressure-modified rate equation, has been compared to finite element simulations using the Eindhoven Glassy Polymer (EGP) constitutive model. Although both methods give quantitatively similar results for the yield stress prediction, only the fully 3D EGP model is able to represent the large-strain deformation behavior.

1 | INTRODUCTION

Acrylonitrile–butadiene–styrene (ABS) is an important engineering co-polymer for industrial and consumer applications. It is used for automotive trim components, enclosures for electrical and electronic equipment, in the construction sector as sheets and pipes, and in household appliances and consumer goods, such as toys, sports and leisure goods, luggage cases, etc.[1] Among its advantages are good mechanical properties for a relative low price compared to other engineering plastics,[2] high surface gloss, and good impact toughness. ABS dominates the market for engineering polymers, accounting for ±41% of the total demand in 2021.[1]

ABS is a rubber-toughened thermoplastic. It consists of a glassy styrene–acrylonitrile (S-AN) co-polymer matrix in which rubber polybutadiene (PB) particles, grafted with styrene and acrylonitrile, are distributed. Volume fraction, particle size, particle size distribution, degree of grafting of the elastomer phase, as well as the component distribution and molecular weight of the glassy matrix can be varied, influencing mechanical properties and deformation behavior.[3–13]

For practical use in polymer solid mechanics, the maximum stress in engineering stress–strain curves in standard tensile experiments at nominal strain rate, i.e. the Ultimate Tensile Strength (UTS), is generally considered as the yield stress. From a mechanical point of view, it is a critical stress value for several reasons: (i) It

is a macroscopic indication of the onset of plastic strain localization.[14–17] This is the moment that localization phenomena initiate, such as necking, shear banding, or crazing. And its known to govern the macroscopic deformation and failure behavior of polymers. At the yield point, the material loses its mechanical integrity and is regarded to fail.[18] (ii) It may be considered as the "limit" where the visco-elastic region ends and the visco-elasto-plastic region begins. Although, it was demonstrated that the true yield point corresponding to the beginning of plastic deformation, as determined via residual strain measurements after unloading, does generally not coincide with the maximum stress in the stress–strain curve.[19] Nevertheless, its value was always close to the maximum stress, and for practical reasons, in the present paper we will consider the maximum stress as the yield stress. (iii) It is not only associated with short-term failure as seen in standard tensile, shear or compression tests, but also with long-term failure in creep or fatigue experiments.[17,20–23]

Thus, a quantitative prediction of the yield stress is an important and significant aspect in order to be able to correctly and safely design a polymer product. It can help to prevent premature failure of, for example, assembly clips, as often used in the automotive industry. In order to obtain usable predictive results, one must therefore consider that Acrylonitrile-Butadiene-Styrene is a time-dependent material, similar to other polymers. Hence, its mechanical response is influenced by strain-rate, temperature, pressure, aging time, etc.,[4,5,24] manifested by a change in yield stress. Various research groups have measured the strain-rate and temperature dependence of different ABS grades.[5,8,9,25,26] It was shown that it was well captured with an Eyring-type flow equation. Furthermore, the influence of hydrostatic pressure on the mechanical properties of ABS has also been a topic of interest over the years. On the one hand, the effects of superimposed high environmental pressure on the mechanical behavior was investigated.[24,27,28] These publications showed that applying high pressures may result in a change of failure mechanism and provoke a pressure-induced brittle-to-ductile transition. On the other hand, pressure-dependence was shown to manifest itself also due to differences in the hydrostatic part of the stress state under different loading geometries, i.e. planar and uniaxial tensile, pure shear, planar and uniaxial compression tests.[29] By converting yield stress data as a function of strain rate into a plot of equivalent shear stress versus equivalent shear rate, this pressure-dependence was visualized. If pressure dependence does not play a role, such curves for different loading geometries will coincide. That is, there would be no difference between the yield stresses and the strain-rate dependence would

be identical. However, for a neat epoxy resin, Govaert et al.[29] showed that the shear data (with a zero hydrostatic part) were above the extensional data (with a positive hydrostatic part) and below the compression data (with a negative hydrostatic part). Furthermore, all curves showed different strain-rate dependence. This indeed demonstrates the effect of the material's pressure dependence.[29,30] This pressure-dependence under different loading geometries (uniaxial tensile, shear, uniaxial compression) was also demonstrated for ABS polymers.[8,25] In the present paper, we only consider pressure-dependence due to different stress states (tensile and compression) in which the hydrostatic pressure does not exceed 30 MPa. This is a pressure range where the yield stress should depend linearly on pressure.[6,19]

Of course, if one should only be performing tensile tests for mechanical characterization of the material, the pressure-dependence would not be detected. Most polymer components undergo a complex stress state in service life, though, with variations along the product. Consequently, from a modeling point of view, it is important to be able to accurately describe the material's behavior in different loading conditions.

In an engineering approach, a description of the yield stress is often sufficient. It was proven by several research groups that an Eyring-type pressure-modified rate equation is able to quantitatively predict the yield stress of several polymers under different loading conditions.[29–33] However, in order to determine the more complex three-dimensional stress state, there is a need for a full three-dimensional model. Several validated models are available[14,34,35] for numerically simulating the large-strain mechanical response of polymer materials using, for example, finite element methods.

In addition, simulation techniques are available to predict the deformation behavior of heterogeneous polymeric systems, such as rubber-toughened thermoplastics. These are generally based on a homogenization method that uses the microstructural morphology to couple, in a numerical way, the microscopic and macroscopic stress–strain behavior. This technique is known as a multilevel finite element method.[36] It has been successfully applied to shed light on the basics of toughness enhancement of polymers through the addition of rubber particles or voids.[37–39] Since the objective of the present paper is not to determine the best combination of volume fraction, particle size, and particle size distribution of the elastomer phase, but rather a design environment for a given or selected polymer, a continuum modeling approach is adopted here.[35]

In the present paper, the focus is on a characterization method for a commercial grade ABS. It nourishes an engineering design environment for the development of

polymer components. It is based on measuring the strain-rate dependence of the material in only two different loading geometries, i.e. uniaxial extension and uniaxial compression, in order to take the pressure-dependence into account. Once that pressure-dependence is determined, other loading conditions and multiaxial stress states can be adequately simulated.[29–33]

As far as the authors know, different commercial or noncommercial ABS grades have been measured over a range of strain rates in a single loading geometry,[3,5,8,9,13,25,26,40] or in different loading geometries (uniaxial tensile, simple shear, uniaxial compression) at a single strain rate.[8,25] However, the strain-rate dependence in various loading geometries has not been found. Since pressure-dependence is an important aspect to simulate multiaxial stress states in polymers, the various methodologies to experimentally determine this aspect will be revised. It will be shown that the method presented here can be an effective one, especially if data under increasing superimposed hydrostatic pressure are not available. The latter type of measurements is more complex and has a need for special equipment.[24,27,28] As shown previously,[29,41,42] the method used here is a general one and can easily be applied to other polymers.

Furthermore, an engineering approach that is based on the yield stress prediction, i.e. a yield criterion, is compared to finite element simulation results with a full three-dimensional constitutive model. It turns out that qualitatively both approaches give similar predictions, but differences do exist that may affect long-term failure in creep or fatigue.

2 | EXPERIMENTAL

2.1 | Acrylonitrile–butadiene–styrene

A commercial injection-molding grade of ABS, ABS Magnum™ 8434 (Styron Netherlands B.V.), was used for the present study. It is widely used for automotive interior trim components. It has a density of 1.05 g cm^{-3} (ISO 1183/B) and a melt flow index (MFI) of 13 g (10 min)$^{-1}$ (ISO 1133). The material has a Butadiene content of $\pm10\%$ and a S–AN ratio of 1:1, as measured with a NMR technique. Before processing, the ABS granules were dried at 80 °C for a minimum of 4 h in a DSN560HE dehumidifier (PIOVAN).

2.2 | Injection molding

Cylindrical tensile bars were injection molded with a Victory 110 injection molding machine (Engel GmbH), with
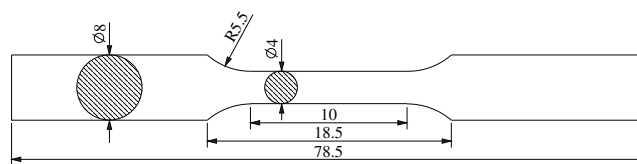

FIGURE 1 Cylindrical tensile test specimen dimensions in [mm]

a clamping force of 1100 kN. Sample dimensions are given in Figure 1. The melt temperature was set to 250 °C, the mold temperature was 60 °C, and a flow rate of 70 cm^3 s^{-1} was used for mold filling. A holding pressure of 60 MPa was applied during 10 s to minimize shrinkage and flash. The cooling time was equal to 30 s.

2.3 | Mechanical characterization

An MTS Criterion C43.104 universal test system, equipped with a 10 kN load cell, was used to determine tensile stress–strain curves. All experiments were performed at room temperature (23 °C). For the uniaxial tensile tests, nominal strain rates ($\dot{\varepsilon}_0 = v/L_0$) were applied in the range from 10^{-4} to 10^{-1} s^{-1}. Three test samples were used for every single strain rate. Yield stresses were determined by taken the maximum stress values in the stress–strain curves, just prior to the occurrence of sample necking. Engineering yield stresses ($\sigma_{y,\,e} = F_{\max}/A_0$) were converted to values for true yield stresses by assuming that the material volume remains constant during uniaxial tensile testing up to yield. This is standard in polymer engineering,[31,43] and according to Govaert et al.[42] it introduces a small error of $\pm2\%$ compared to a compressible approach.

For uniaxial compression tests, cylindrical samples with a diameter and height of 6 mm were machined from the injection mold runners (8 mm initial diameter). The samples were compressed between two parallel flat steel platens, mounted in the same MTS Criterion C43-104 universal test system. To reduce friction in order to avoid bulging or buckling of the samples, a thin PTFE skived film tape (3M 5480) was attached to the sample ends and the surface between steel platens and tape was lubricated with a PTFE spray. Homogeneous deformation during the complete compression test range was observed, indicating that friction was sufficiently reduced. Nominal strain rates ($\dot{\varepsilon}_0 = v/L_0$) ranging from from 3×10^{-4} to 10^{-1} s^{-1} were applied at room temperature. Three test samples were used for every single strain rate. Since homogeneous deformation was obtained during testing, even at large strains, true stress–strain curves can be directly determined from the uniaxial compression tests

TABLE 1 Definitions of the equivalent (plastic) shear rate, $\dot{\bar{\gamma}}$, shear stress, $\bar{\tau}$, and hydrostatic pressure, p, expressed in components of the deformation and stress tensor. Explicit expressions are given for tension, compression, and shear

Definition	Tension	Compression	Shear
$\dot{\bar{\gamma}} = \sqrt{2\left(\dot{\varepsilon}_{11}^2 + \dot{\varepsilon}_{22}^2 + \dot{\varepsilon}_{33}^2 + 2\dot{\varepsilon}_{12}^2 + 2\dot{\varepsilon}_{13}^2 + 2\dot{\varepsilon}_{23}^2\right)}$	$\sqrt{3}\dot{\varepsilon}$	$\sqrt{3}\,\lvert\dot{\varepsilon}\rvert$	$\dot{\gamma}$
$\bar{\tau} = \sqrt{\frac{1}{6}\left[(\sigma_{11} - \sigma_{22})^2 + (\sigma_{22} - \sigma_{33})^2 + (\sigma_{33} - \sigma_{11})^2\right] + \sigma_{12}^2 + \sigma_{13}^2 + \sigma_{23}^2}$	$\frac{\sigma}{\sqrt{3}}$	$\frac{\lvert\sigma\rvert}{\sqrt{3}}$	τ
$p = -\frac{1}{3}(\sigma_{11} + \sigma_{22} + \sigma_{33})$	$-\frac{\sigma}{3}$	$+\frac{\lvert\sigma\rvert}{3}$	0

under the assumption of incompressibility and applying a correction for the machine set-up stiffness.

2.4 | Numerical simulations

The structural analysis simulations were performed using the commercial finite element package MSC.Marc, version 2005r3. The constitutive 3D elasto-viscoplastic Eindhoven Glassy Polymer (EGP) model (see next section) was implemented by means of the HYPELA2 user subroutine. Only the part between the test set-up clamps was meshed and analyzed in the simulations. Uniaxial compression tests were simulated axi-symmetrically using a single linear quad4 element. Uniaxial tensile tests were also simulated in an axi-symmetric way, by meshing only half of the part between clamps using 1357 linear quad4 elements.

3 | MODELING

In this section, two modeling methods will be presented to describe the deformation behavior for commercial polymer grades. The first one is an engineering approach that basically is a yield criterion for describing yield stresses only. The second one is a full three-dimensional model, able to capture more complex large-strain multi-axial stress states.

3.1 | Pressure-dependent Ree-Eyring flow rule

The deformation kinetics of polymer materials can be well characterized by a linear dependence of the yield stress on the logarithm of strain rate, the temperature, and the pressure, as has been shown over the years.[29–31,43–46] For polymers with a thermorheologically simple response,[44] an Eyring-type pressure-modified rate equation[30] can quantitatively capture the yield stress behavior:

$$\dot{\bar{\gamma}}(T,\bar{\tau},p) = \dot{\gamma}_0 \exp\left(-\frac{\Delta U}{RT}\right)\exp\left(-\frac{\mu p V^*}{kT}\right)\sinh\left(\frac{\bar{\tau}V^*}{kT}\right) \quad (1)$$

Here, $\dot{\bar{\gamma}}$ is the equivalent plastic shear rate, T the absolute temperature in K, $\bar{\tau}$ the equivalent shear stress, p the hydrostatic pressure, $\dot{\gamma}_0$ a rate constant, ΔU the activation energy ($257\,\text{kJ}\,\text{mol}^{-1}$, as taken from literature[5]), R the universal gas constant ($8.314472\,\text{J}\,\text{mol}^{-1}\,\text{K}^{-1}$), μ a pressure dependence parameter, V^* the activation volume, and k is the Boltzmann's constant ($1.38054 \times 10^{-23}\,\text{J}\,\text{K}^{-1}$). Definitions for the equivalent plastic shear rate $\dot{\bar{\gamma}}$ (based on the second invariant of the rate of strain tensor), equivalent shear stress $\bar{\tau}$ (based on the second invariant of the deviatoric stress tensor), and hydrostatic pressure p are given in Table 1. Expressions for uniaxial tension, uniaxial compression, and pure shear are also given in Table 1, and show that the equivalent stress and shear rate are equal to the values measured in a pure shear test.

The prefix $\dot{\gamma}_0$ is a rate constant that reduces with diminished molecular mobility.[47] It depends on the thermodynamic state of the material and is related to the density increase due to physical aging,[35] which restricts molecular mobility. As a consequence, yield stresses augment. The first exponential term, which includes the activation energy ΔU, covers the material's temperature dependence. It is related to the potential energy barrier that needs to be exceeded for segmental motion (i.e. molecular conformational changes). The last term, a hyperbolic sine function that includes the activation volume V^*, determines the stress dependency of the material. The stress in combination with the activation volume regulates the decrease of the potential energy barrier for segmental motion in the direction of the applied stress.[48] V^* can be interpreted as a volume that is involved in a plastic deformation mechanism, and is related to the size of several statistical random links in the polymer chain that move simultaneously in a cooperative way.[30,49] The second exponential term, which includes the pressure dependence parameter μ, captures the effect of hydrostatic pressure. A negative hydrostatic pressure, for example, as encountered in a tensile test experiment, lowers the potential energy barrier for

molecular conformational changes. Contrary, a positive hydrostatic pressure (e.g., during compression tests) increases this potential energy barrier. The higher the parameter μ, the bigger the effect of hydrostatic pressure and the bigger the difference between tensile and compression data. Therefore, Equation (1) can be used to evaluate (in a macroscopic sense) the potential energy barriers involved in the plastic deformation mechanisms at the yield stress, and the effects of temperature, strain rate, and pressure on those energy barriers.

If written in terms of the equivalent shear stress as a function of equivalent shear rate, the equation reads:

$$\overline{\tau}(T,\dot{\overline{\gamma}},p) = \frac{kT}{V^*}\sinh^{-1}\left[\frac{\dot{\overline{\gamma}}}{\dot{\gamma}_0}\exp\left(\frac{\Delta U}{RT}\right)\exp\left(\frac{\mu p V^*}{kT}\right)\right]. \quad (2)$$

Yet, many polymers exhibit two (or even more) molecular relaxation processes. Transitions, for example, due to a change in temperature or deformation rate, occur when a certain molecular relaxation process starts to manifest itself or, on the contrary, ceases to materialize. These transitions can become visible in yield stress versus logarithmic strain-rate plots and generally manifest themselves by a change in the slope in these plots.[43] This behavior is termed as thermorheologically complex behavior. In these cases, the yield behavior can be well described by the Ree-Eyring modification[50] of the Eyring-type flow rule, assuming that different molecular processes act independently and in parallel:

$$\overline{\tau}(T,\dot{\overline{\gamma}},p) = \sum_{x=\alpha}^{\delta}\frac{kT}{V_x^*}\sinh^{-1}\left[\frac{\dot{\overline{\gamma}}}{\dot{\gamma}_{0,x}}\exp\left(\frac{\Delta U_x}{RT}\right)\exp\left(\frac{\mu_x p_x V_x^*}{kT}\right)\right]. \quad (3)$$

Here, x relates to the indication of the parameters related to each relaxation process, customarily labeled in polymers as α, β, γ, δ, etc. with decreasing temperature.[51] Commonly, the molecular processes are related to the main-chain segmental motion (the primary glass- or α-transition) and a partial side-chain mobility (a secondary or β-transition).[47] Nonetheless, for a poly(methyl methacrylate) polymer, De Deus et al.[51] have encountered even four molecular relaxation processes.

By making use of the expressions in Table 1, the pressure-dependent Ree-Eyring flow rule (Equation (3)) can be simplified to describe the true yield stresses for both tensile as well as compression tests. This results for the uniaxial tensile tests in:

$$\sigma_y^{\text{tens}} = \sum_{x=\alpha}^{\delta}\frac{3}{\sqrt{3}+\mu_x}\frac{kT}{V_x^*}\sinh^{-1}\left[\frac{\sqrt{3}\dot{\varepsilon}}{\dot{\gamma}_{0,x}}\exp\left(\frac{\Delta U_x}{RT}\right)\right], \quad (4)$$

while for the uniaxial compression tests in:

$$|\sigma_y^{\text{comp}}| = \sum_{x=\alpha}^{\delta}\frac{3}{\sqrt{3}-\mu_x}\frac{kT}{V_x^*}\sinh^{-1}\left[\frac{\sqrt{3}|\dot{\varepsilon}|}{\dot{\gamma}_{0,x}}\exp\left(\frac{\Delta U_x}{RT}\right)\right]. \quad (5)$$

Note that the only difference resides in the opposite sign for the hydrostatic pressure parameter μ_x. This not only accounts for a difference between the yield stress under different loading geometries, but also for a distinct strain-rate dependence. Note also that true stress values are referred to in the previous equations.

3.2 | Full 3D constitutive equation

As a constitutive model for the material behavior, the multi-mode multi-process 3D elasto-viscoplastic Eindhoven Glassy Polymer (EGP) model[35,47,52,53] is given, known to accurately capture the intrinsic large-strain deformation characteristics of polymeric glasses. The basis of the EGP-model is the split of the Cauchy stress into a hardening stress, σ_r, and a driving stress, σ_s, first proposed by Haward and Thackray[49]:

$$\sigma = \sigma_r + \sigma_s \quad (6)$$

The strain hardening contribution is attributed to the molecular orientation of the entangled polymer network and is modeled by a Neo-Hookean elastic expression:

$$\sigma_r = G_r\widetilde{\boldsymbol{B}}^d, \quad (7)$$

consisting of the strain-hardening modulus G_r and the deviatoric part of the isochoric left Cauchy-Green strain tensor $\widetilde{\boldsymbol{B}}$. The driving stress, attributed to intermolecular interactions on a segmental scale, is decomposed into a hydrostatic part and a deviatoric part, representing the volumetric change and the rate-dependent plastic flow, respectively. The deviatoric driving stress is split into contributions for varios molecular processes[47] (in this case only two, α and β), each modeled by a non-linear multi-mode Maxwell model[52,53]:

$$\begin{aligned}\sigma_s &= \sigma_s^h + \sigma_{s,\alpha}^d + \sigma_{s,\beta}^d \\ &= \kappa(J-1)\boldsymbol{I} + \sum_{i=1}^{n}G_{\alpha,i}\widetilde{\boldsymbol{B}}_{e,\alpha,i}^d + \sum_{j=1}^{m}G_{\beta,j}\widetilde{\boldsymbol{B}}_{e,\beta,j}^d.\end{aligned} \quad (8)$$

Here, κ is the bulk modulus, J the volume change ratio, $\boldsymbol{I}$ the unity tensor. $G_{x,i}$ is a shear modulus of the ith

(related to the α-process) or the jth mode (related to the β-process). The evolution equations of the volumetric (J) and elastic strains ($\widetilde{\boldsymbol{B}}_{e,x}$) of the different modes are given by:

$$\dot{J} = J\,\mathrm{tr}(\boldsymbol{D}), \tag{9}$$

$$\dot{\widetilde{\boldsymbol{B}}}_{e,\alpha,i} = \left(\widetilde{\boldsymbol{L}} - \boldsymbol{D}_{p,\alpha,i}\right) \cdot \widetilde{\boldsymbol{B}}_{e,\alpha,i} + \widetilde{\boldsymbol{B}}_{e,\alpha,i} \cdot \left(\widetilde{\boldsymbol{L}}^c - \boldsymbol{D}_{p,\alpha,i}\right), \tag{10}$$

$$\dot{\widetilde{\boldsymbol{B}}}_{e,\beta,j} = \left(\widetilde{\boldsymbol{L}} - \boldsymbol{D}_{p,\beta,j}\right) \cdot \widetilde{\boldsymbol{B}}_{e,\beta,j} + \widetilde{\boldsymbol{B}}_{e,\beta,j} \cdot \left(\widetilde{\boldsymbol{L}}^c - \boldsymbol{D}_{p,\beta,j}\right), \tag{11}$$

where $\widetilde{\boldsymbol{L}}$ is the isochoric velocity gradient tensor, and $\boldsymbol{D}_{p,x,i}$ is the plastic part of the rate of deformation tensor $\boldsymbol{D}$ belonging to process x and mode i, defined as:

$$\boldsymbol{D}_{p,x,i} = \frac{\boldsymbol{\sigma}_{s,x,i}^d}{2\eta_{x,i}(T,\overline{\tau}_x,p_x,S_x)}. \tag{12}$$

The viscosities $\eta_{x,i}$ are based on an Eyring equation, modified to take pressure (p_x) and intrinsic strain softening (S_x) into account:

$$\eta_{x,i} = \eta_{0,x,i,\mathrm{ref}}\exp\left(\frac{\Delta U_x}{R}\left[\frac{1}{T} - \frac{1}{T_{ref}}\right]\right)\frac{\overline{\tau}_x/\tau_{0,x}}{\sinh(\overline{\tau}_x/\tau_{0,x})} \\ \times \exp\left(\frac{\mu_x p_x}{\tau_{0,x}}\right)\exp(S_x), \tag{13}$$

where $\eta_{0,x,i,\mathrm{ref}}$ is the zero viscosity of the ith relaxation mode in the rejuvenated state at the reference temperature, ΔU_x the activation energy for the temperature dependence, $\overline{\tau}_x$ is the total equivalent stress, $\tau_{0,x}$ is a characteristic stress, and S_x is the thermodynamic state parameter that captures the effect of physical aging and strain softening, all related to molecular process x. R is the gas constant, and T_{ref} the reference temperature in K. The total equivalent stress, the characteristic stress, and the hydrostatic pressure for process x are defined as:

$$\overline{\tau}_x = \sqrt{\frac{1}{2}\boldsymbol{\sigma}_{s,x}^d : \boldsymbol{\sigma}_{s,x}^d}, \quad \tau_{0,x} = \frac{kT}{V_x^*}, \quad p_x = -\frac{1}{3}\mathrm{tr}(\boldsymbol{\sigma}_{s,x}), \tag{14}$$

where V_x^* is the activation volume for process x.

The thermodynamic state parameter S_x is composed of two contributions, which are assumed to be fully decoupled:

$$S_x\left(t,T,\overline{\gamma}_{p,x}\right) = S_{a,x}\cdot R_x\left(\overline{\gamma}_{p,x}\right), \tag{15}$$

where $S_{a,x}$ represents the current thermodynamic state of each process, which is usually a constant for short-term experiments. $R_x\left(\overline{\gamma}_{p,x}\right)$ is the softening function as a result of mechanical rejuvenation determined by the equivalent plastic strain $\overline{\gamma}_{p,x}$. The softening function $R_x\left(\overline{\gamma}_{p,x}\right)$ is described using a modified Carreau-Yasuda expression that is normalized to 1 and decreases monotonically to 0 with increasing (equivalent) plastic strain. Following Van Breemen et al.,[47] the softening function only depends on the molecular process with the longest relaxation times, which belongs to the α-process. This leaves the softening function to read:

$$R_x\left(\overline{\gamma}_{p,\alpha}\right) = \frac{\left(1 + \left[r_{0,x}\cdot\exp\left(\overline{\gamma}_{p,\alpha}\right)\right]^{r_{1,x}}\right)^{(r_{2,x}-1)/r_{1,x}}}{\left(1 + r_{0,x}^{r_{1,x}}\right)^{(r_{2,x}-1)/r_{1,x}}}, \tag{16}$$

where $r_{0,x}$, $r_{1,x}$, and $r_{2,x}$ are fitting parameters for process x ($x = \alpha, \beta$). The plastic strain evolution is coupled to the longest relaxation time, that is, mode $i = 1$ of process α, and defined as:

$$\dot{\overline{\gamma}}_{p,\alpha} = \frac{\overline{\tau}_{\alpha,1}}{\eta_{\alpha,1}}, \text{where} \quad \overline{\tau}_{\alpha,1} = \sqrt{\frac{1}{2}\boldsymbol{\sigma}_{s,\alpha,1}^d : \boldsymbol{\sigma}_{s,\alpha,1}^d}. \tag{17}$$

Again, the previous equations use true stresses.

3.3 | Hydrostatic pressure influence

Let us assume the general case where a polymer material demonstrates thermorheologically complex behavior. Moreover, it is also assumed that the pressure dependence μ is different for the multiple molecular relaxation processes, that is, μ_x for process x ($x = \alpha, \beta, \gamma, \delta$).

Now, a direct method to determine the hydrostatic pressure influence on the deformation kinetics of polymer materials, is by performing experiments under increasing superimposed hydrostatic pressure.[24,27,28] The main advantage is that the pressure dependence parameter μ_x can be directly established from the data displaying the yield stress as a function of superimposed hydrostatic pressure. However, these kind of measurements are rather complex and have the need of special equipment.[24,27] Furthermore, the data obtained with these kind of measurements should be considered with care. It was indicated, for example, by Vroom and Westover,[27] that certain pressure media may act as a plasticizer, affecting the data. To prevent the possible entry of the pressure medium into the polymer, some authors apply coating to the specimen.[28,54] As a

consequence, it adds another complication to these kind of experiments.

By lack of data from experiments under superimposed hydrostatic pressure, another common way to determine the pressure dependence μ is via the difference in yield stresses obtained in different loading geometries (e.g., uniaxial tension, uniaxial compression, pure shear, torsion, planar tension, etc.). This method has been applied by various research groups over the years.[19,23,30,31,55–57] If uniaxial tension (superscript tens) and compression (superscript comp) tests are used, as is the case in the present paper, the pressure dependency μ_x for molecular process x then reads:

$$\mu_x = \sqrt{3} \cdot \frac{|\sigma_{y,x}^{comp}| - \sigma_{y,x}^{tens}}{|\sigma_{y,x}^{comp}| + \sigma_{y,x}^{tens}}. \tag{18}$$

However, this implies that the previous equation is independent of the strain rate and, as was mentioned by Ward,[30] this is generally not true. For tests with different loading geometries, distinct sample shapes and dimensions are required. Varying dimensions influences the thermal history during processing, provoking a change in the thermodynamic state of the resulting component.[58,59] As a consequence, the mechanical properties, that is, the yield stresses, also change. This means, that for different thermodynamic states, different values of μ_x will be the result. In order for Equation (18) to be valid, it is essential to obtain test specimen with identical states. This was pointed out by Klompen et al.[35]

Even so, as was shown by, for example, Bauwens-Crowet and Bauwens[60] and Klompen et al.,[17] sample sets with different thermodynamic states show significantly altered yield stresses, but an unaffected strain rate dependence. The same holds for measuring at various temperatures, provided that there are no changes in the molecular relaxation processes in the strain rate range.[44,60] This implies that the same activation volume V_x^* is involved for testing samples with distinct thermodynamic states or temperatures.[60] Furthermore, yield stresses obtained in different loading geometries, demonstrate dissimilar strain rate dependence.[29–32,42,53] Hence, a third alternative presents itself to determine the pressure dependency μ_x. It is based on this difference in slopes on the curves representing the yield stress as a function of logarithmic strain rates ($\sigma_y - \log(\dot{\varepsilon})$) for different loading geometries. If uniaxial tensile (superscript tens) and compression (superscript comp) tests are used, the pressure dependency μ_x then reads:

$$\mu_x = \sqrt{3} \cdot \frac{T^{tens}\left(|\sigma_{y,x,2}^{comp}| - |\sigma_{y,x,1}^{comp}|\right) - T^{comp}\left(\sigma_{y,x,2}^{tens} - \sigma_{y,x,1}^{tens}\right)}{T^{tens}\left(|\sigma_{y,x,2}^{comp}| - |\sigma_{y,x,1}^{comp}|\right) + T^{comp}\left(\sigma_{y,x,2}^{tens} - \sigma_{y,x,1}^{tens}\right)}. \tag{19}$$

Here, subscript 2 refers to the yield stress at the highest measured strain rate equal for both loading geometries, while subscript 1 to the lowest measured strain rate. Note that the temperature drops out, if data is selected at the same temperature for both tension and compression. However, taking data at different temperatures may be beneficial in case of materials with multiple molecular relaxation processes.

As was already shown by Bauwens-Crowet,[41] Equation (19) can also be written in terms of activation volumes, since those are related to the slope of the yield stress as a function of logarithmic strain rate. The pressure dependency μ_x then reads:

$$\mu_x = \sqrt{3} \cdot \frac{V_x^{*,tens} - V_x^{*,comp}}{V_x^{*,tens} + V_x^{*,comp}} \tag{20}$$

Here, $V_x^{*,tens}$ and $V_x^{*,comp}$ are the activation volumes for process x if no pressure dependence is taken into account for the uniaxial tensile and compression data, respectively. Compare this Equation (20) to Equations (4) and (5), and note again that the hydrostatic pressure parameter μ_x accounts for the difference in strain-rate dependence of the yield stress under different loading geometries. This alternative third method has been successfully applied previously for several polymers.[29,41,42]

4 | RESULTS

4.1 | Engineering approach

The experimental results for the uniaxial compression tests at various strain rates for this ABS Magnum™ 8434 are given in Figure 2a. The upper and lower yield stresses, as well as the yield drop, as a function of logarithmic nominal strain rate are demonstrated in Figure 2b. At the highest strain rate, that is, $\dot{\varepsilon} = 10^{-1} \text{ s}^{-1}$, the sample is affected by viscous heating at large deformations. This is visible due to a strong reduction in strain hardening at higher strains, leading to a crossover with the curve at a lower strain rate. This effect was previously reported by other research groups.[47,61]

Following the method exposed by Van Breemen et al.,[47] a material's thermorheologically complex behavior can be detected by different strain-rate dependence of the upper and lower yield stresses. This may be the case for the ABS used in the present study, as would suggest the data of Figure 2b in the strain-rate range 3×10^{-4} to 10^{-2} s^{-1}. Nevertheless, by revising dynamical mechanical analysis (DMA) data from literature,[3,62–64] another scenario may be more plausible. The α-transition of the S-

AN matrix, that is, the glass transition temperature T_g of ABS, is consistently measured around 115 °C. The α-transition of the rubber PolyButadiene particles is generally detected below −50 °C. Occasionally, but not always, a β-transition of the S-AN phase has been measured at around −15 °C.[63] Hence, there is a rather large temperature difference between the α- and the β-transition for it to become visible in the strain-rate range as measured here. For such a large temperature difference, comparable to polycarbonate, generally only one molecular relaxation process is visible.[44,47] In order to detect the β-transition, sufficiently low temperatures and/or high strain rates need to be assessed.[31] Furthermore, ABS data as measured over a strain-rate range for higher[9] and lower temperatures,[5] did not indicate any secondary molecular relaxation mechanism.

Based on the above findings, it is therefore thought that viscous heating is also affecting the uniaxial compression data at $\dot{\varepsilon} = 10^{-2}$ s^{-1}. Although much more

difficult to detect than for the highest measured strain rate, the strain hardening at 10^{-2} s^{-1} is slightly reduced compared to the lowest strain rates. Besides, the strain at which the lower yield stress is detected, is shifted toward a higher strain: $\varepsilon \approx 0.30$ for $\dot{\varepsilon} = 10^{-2}$ s^{-1} versus $\varepsilon \approx 0.26$ for both $\dot{\varepsilon} = 10^{-3}$ s^{-1} and 3×10^{-4} s^{-1}. This shift is another indication of possible viscous heating.

For uniaxial tensile tests, engineering stress/strain curves ($\sigma_e = F/A_0$, $\varepsilon_e = \Delta L/L_0$) at several strain rates are depicted in Figure 3a. This data, converted into true yield stress as a function of logarithmic nominal strain rate, is compared to the uniaxial compression experiments in Figure 3b. These tensile results clearly show the thermorheologically simple behavior of ABS Magnum™ 8434 at this temperature and over the measured strain-rate range. Therefore, the pressure-dependent Eyring flow rule using only a single molecular deformation process, that is, the α-process, is sufficient to describe the data.
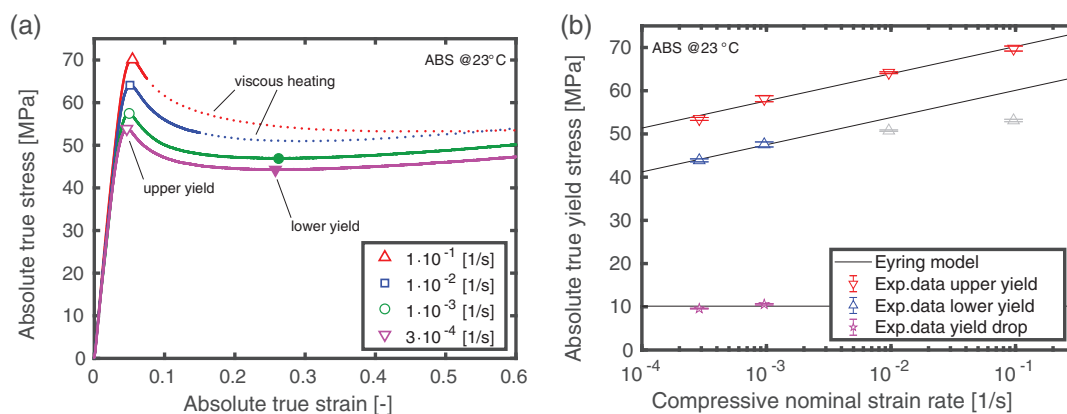

FIGURE 2 (a) Experimental absolute true stress/strain response in compression at various strain rates. (b) Absolute true upper (▽) and lower (△) yield stresses, and yield drop (⋆) as a function of decimal logarithmic strain rate. Symbols are experimental data, solid lines are model predictions. Gray symbols are data affected by viscous heating [Color figure can be viewed at wileyonlinelibrary.com]
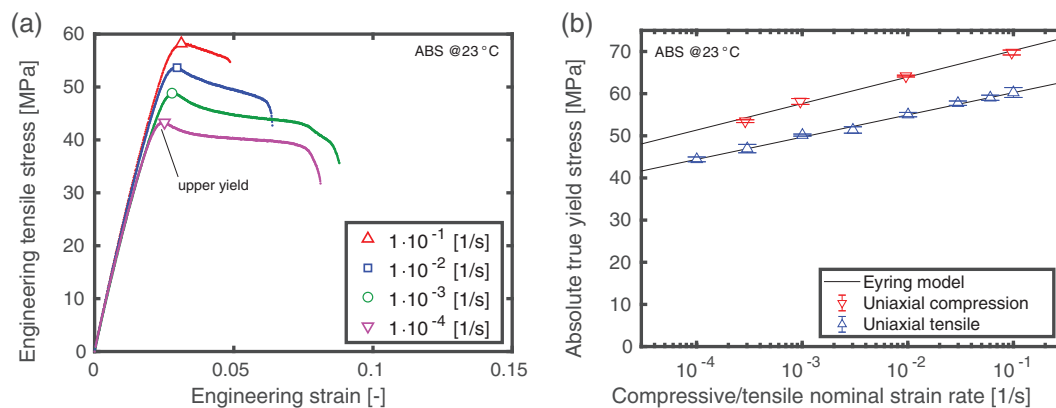

FIGURE 3 (a) Experimental engineering stress/strain response in tension at various strain rates. (b) Absolute true yield stresses as a function of decimal logarithmic strain rate in compression and tension. Symbols are experimental data, solid lines are model predictions [Color figure can be viewed at wileyonlinelibrary.com]
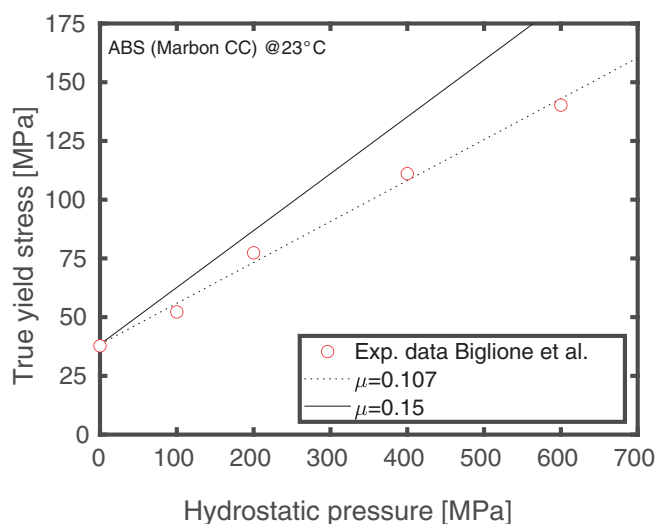
FIGURE 4 True yield stress as a function of hydrostatic pressure in tension. Experimental data are adopted from Biglione et al.[24] Symbols are experimental data, lines are model predictions [Color figure can be viewed at wileyonlinelibrary.com]

TABLE 2 Eyring model parameters for ABS material

	Superimposed hydrostatic pressure	Different slopes compression/ tension
μ [−]	0.107	0.15
V^* [nm^3]	2.76	2.84
$\Delta U^{a)}$ [kJ mol^{-1}]	257	257
$\dot{\gamma}_0^{comp}$ [s^{-1}] (upper yield)	$5.09 \cdot 10^{33}$	$5.09 \cdot 10^{33}$
$\dot{\gamma}_0^{comp}$ [s^{-1}] (lower yield)	$2.08 \cdot 10^{35}$	$2.08 \cdot 10^{35}$
$\dot{\gamma}_0^{tens}$ [s^{-1}] (tension)	$9.10 \cdot 10^{33}$	$3.00 \cdot 10^{33}$

[a]Data taken from Truss & Chadwick.[5]

To determine the pressure dependence of the material, tensile data under superimposed hydrostatic pressure was taken from Biglione et al.[24] Experimental results are shown as symbols in Figure 4. The particular ABS material used for their experiments was a commercial grade from Marbon Chemical Company,[24] containing 20% Butadiene in a S–AN matrix with ratio 2.2:1. Since the composition of this co-polymer is different, it may influence results.

Using the Biglione hydrostatic data, the pressure dependence results in $\mu = 0.107$. The other model parameters are given in the left column of Table 2. The Eyring model predictions using this parameter set are shown as solid lines in Figures 2b and 3b, and as a dashed line in Figure 4. Note that the rate constants for the compression upper yield stress and the tensile yield stress are not the same, although very similar. Hence, this indicates that the thermodynamic state of the samples used for the two measurements is not exactly the same, although taken from the same injection molding sets. Possibly the machining operation needed to obtain the compression samples may have slightly altered experimental results. Machining operations are believed to influence the thermodynamic state of a thin surface layer, thus possibly changing yield stress values a little.[59,65] With proper precautions, this effect can be minimized but never completely eradicated.

If the pressure dependence is calculated by taking the difference between the yield stresses in tension and compression, i.e. according to Equation (18), the result ranges from $\mu_{min} = 0.123$ at low strain rate to $\mu_{max} = 0.134$ at

high strain rate. This confirms the statement in the previous paragraph, that the thermodynamic state of the tensile and compression samples are similar but not completely equal.

Using the third method to determine pressure dependence, i.e. based on the difference in slopes of the $\sigma_y - \log(\dot{\varepsilon})$ curves in tension and compression (according to Equations (19) or (20)), a value of $\mu = 0.15$ is the outcome. The rest of the model parameters are given in the right column of Table 2. The Eyring model now performs very similar to the method using superimposed hydrostatic pressure, resulting in the solid lines in Figures 2b, 3b, and 4. In fact, with this second set of parameters, the Eyring model performs slightly better in tension and compression: a coefficient of determination $R^2 = 0.9832$ as opposed to $R^2 = 0.9806$. It is also mentioned, that the pressure dependence determined here is in the similar range as calculated by Chen & Sauer.[8] The other model parameters are also in comparable ranges as parameters previously published by other research groups.[2,5,8]

Logically, Figure 4 gives a different description for both methods, as this data was not used to determine the second set of Eyring parameters. Furthermore, as mentioned earlier, the composition of the two ABS materials is not the same (10% PB-particles versus 20% PB-particles, different Styrene and Acrylonitrile contents). As was mentioned by Klompen and Govaert,[66] subtle differences in material composition and additives could be one of the causes for parameter value deviations. The exact nature is, however, difficult to determine without further research.

To resume, the third alternative proves to be an effective method, resulting in a very satisfying description of ABS material behavior in tension and compression. Particularly considering that data under increasing

superimposed hydrostatic pressure is not available for this particular grade.

4.2 | Thermorheologically complex response

In the previous subsection, the pressure dependence was determined on an ABS polymer, with data showing thermorheologically simple behavior. To show that the method based on the difference in slopes of the $\sigma_y - \log(\dot{\varepsilon})$ curves in tension and compression is not restricted to these kind of materials, it is also applied to a material with more than one molecular relaxation process. The classical data of Bauwens–Crowet[41] for a commercial grade poly(methyl methacrylate) Perspex ICI (PMMA) is adopted for that purpose, and shown in Figure 5. It is data covering a wide range of temperatures and strain-rates, both in tension and compression, making it an appropriate data test set.

Evaluating closely the data, two distinct changes in the slope of the strain-rate dependent yield stress data can be detected. This means that even three molecular relaxation mechanisms influence the data in the measured range. Bauwens–Crowet already mentioned this and observed a combined peak for a secondary molecular relaxation mechanism in mechanical damping tests (see Figures 6 and 7 of that paper[41]). Although for a different PMMA (from Rohm and Haas Co.), Thompson[67] also detected a third molecular process in creep compliance measurements (see Figure 8 of that paper[67]). Both authors denominated those transitions in PMMA as α, α', and β, which will also be adopted here.

Such a third molecular deformation process has not been noticed in other publications regarding yield stresses as a function of logarithmic strain rate for PMMA.[43,47,66] The reason is that those measurements generally did not reach high enough strain rates and/or low enough temperatures for it to become clearly visible.

The strategy to adjust model parameters is similar to what was described by other authors.[35,41,47] The principal idea is to adjust the parameters region by region, i.e. starting with the α-regime where only a single molecular process is active and ending with the regime with, in this particular case, three processes (α, α', β). Initially, pressure dependence is not taken into account, leading to $\mu_\alpha = 0$. Next, for the data with the lowest strain rates and the highest temperatures (α-regime), the activation volumes $V_\alpha^{*,\,\text{tens}}$ and $V_\alpha^{*,\,\text{comp}}$ are determined from the slopes of the strain-rate dependence ($\sigma_y - \log(\dot{\varepsilon})$ curves) for tension and compression, respectively. Then, an adequate activation energy $\Delta U_\alpha^{\text{tens}} = \Delta U_\alpha^{\text{comp}}$ is established, able to describe the temperature dependence for both tension and compression simultaneously. Last, the rate constants for tension $\dot{\gamma}_{0,\alpha}^{\text{tens}}$ and compression $\dot{\gamma}_{0,\alpha}^{\text{comp}}$ are fixed. Now, the pressure dependence can be determined using Equation (20). The activation volume needs to be recalculated to be the same for both tension and compression using:

$$V_x^* = V_x^{*,\text{tens}} \cdot \frac{\sqrt{3}}{\sqrt{3}+\mu_x} \quad \text{or} \quad V_x^* = V_x^{*,\text{comp}} \cdot \frac{\sqrt{3}}{\sqrt{3}-\mu_x}, \tag{21}$$

where $x = \alpha$.

To adjust parameters for the second molecular process (α'-regime), the model response for the primary process (α-regime) needs to be subtracted from the experimental data. Then, the same steps as explained
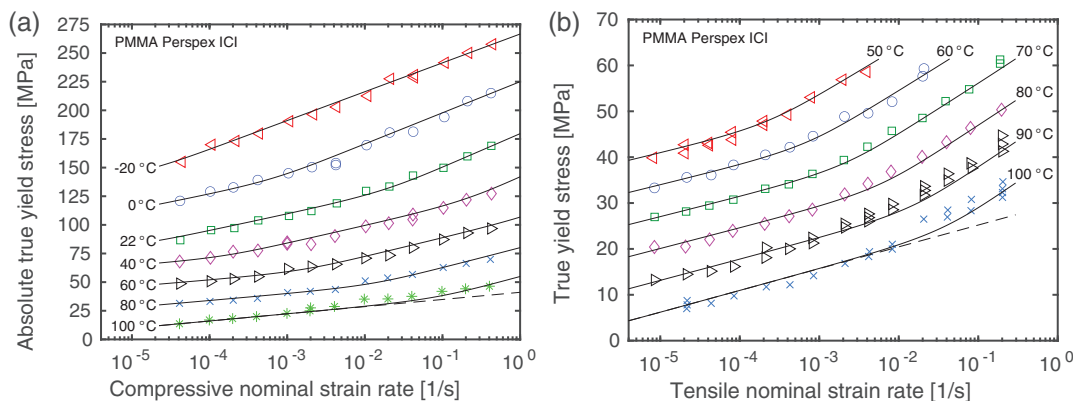

FIGURE 5 *(a)* Compression yield stresses as a function of decimal logarithmic strain rate at various temperatures. *(b)* Tensile yield stresses as a function of decimal logarithmic strain rate at various temperatures. Symbols are experimental data for PMMA adopted from Bauwens-Crowet[41]; solid lines are multi-process model predictions, while dashed lines correspond to a single-process model [Color figure can be viewed at wileyonlinelibrary.com]

above are followed. For compression, data are taken at the intermediate temperature (22°C) and the lowest strain rates, while for tension, data are taken at 70°C and the highest strain rates. For the last molecular process (β-regime), the model responses for both the primary (α) and secondary (α') processes need to be subtracted from the experimental data. As no tensile experimental data are available in this last regime, its pressure dependence can not be determined and is taken as $\mu_\beta = 0$.

The final PMMA model parameters are given in Table 3. Model predictions for the pressure-dependent Ree-Eyring modification of the Eyring flow rule using this parameter set are shown as solid lines in Figure 5. The dashed lines in that figure represent a single-process model. The temperature dependence of the absolute compression yield stress at a single strain rate, as shown in Figure 3 of Bauwens-Crowet's work,[41] can also be excellently predicted with this parameter set (not shown here). Model parameters in Table 3 are close to and in agreement with previously published research.[30,41,49,66] Furthermore, they comply with the physics related to the potential energy barriers involved in the plastic deformation mechanisms at the yield stress.

4.3 | EGP model

Starting with initial values as determined in the engineering approach, the parameters for the 3D elasto-viscoplastic Eindhoven Glassy Polymer (EGP) model were fitted to the uniaxial compression data. The resulting parameter set is given in Table 4. The activation volume V_α^* is very similar to the Ree-Eyring parameter, although slightly different. The EGP model uniaxial compression prediction using the parameter set of Table 4 is shown in Figure 6a. Since viscous heating is not implemented in the model, that effect is not simulated.

By comparing the numerical results with the experiments, however, the effect of viscous heating can be noticed. For strain rate $\dot{\varepsilon} = 10^{-2}$ s^{-1}, the experimental stress/strain curve drops further than the simulated one. As a consequence, the lower yield stress occurs at a higher strain, as mentioned previously. Furthermore, it can also be seen that the experimental strain hardening seems to keep on being parallel to the simulated one. Hence, this makes it difficult to experimentally detect viscous heating.

Without changing the thermodynamic state parameter $S_{a,\alpha}$ (which would provoke a vertical shift of the yield stress prediction similar to a change in the rate constant $\dot{\gamma}_0$), the parameter set as given in Table 4 is used to simulate the uniaxial tensile tests. The engineering stress/strain graphs for various strain rates are demonstrated in Figure 6b. Surprisingly, the height of the yield stresses are excellently predicted. This may indicate that the machining operation to obtain the compression samples may have a negligible effect after all.

The initial post-yield response of the tensile tests is well predicted by the EGP model. Since no failure criterion is implemented in the model, the strain and stress at break are, logically, not captured. Moreover, without a failure criterion, crazing can not be predicted, which is known to be one of the principle failure mechanisms of ABS material.[5] In fact, the tensile experiments demonstrated stress whitening (an indication for crazing phenomena) and hardly any necking before breaking. The simulations, on the contrary, showed considerable necking at large strains. This shortcoming may be the reason that strain hardening seems to be underpredicted by the model in tensile tests. The implementation of a failure
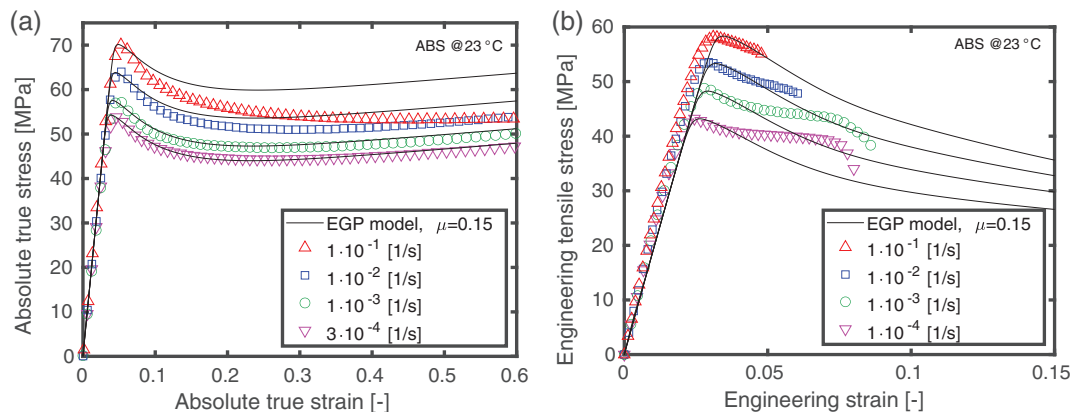

FIGURE 6 (a) Absolute true stress/strain response in compression at various strain rates. (b) Engineering stress/strain response in tension at various strain rates. Symbols are experimental data; solid lines are EGP model predictions [Color figure can be viewed at wileyonlinelibrary.com]

criterion is, however, beyond the scope of the present study.

The description of the EGP model for the $\sigma_y - \log(\dot{\varepsilon})$ behavior is equal to the Eyring model predictions as displayed in Figures 2b and 3b. Therefore, these models are well capable of describing the deformation behavior of ABS material simultaneously in both compression and tension.

An equally good description of the compression tests could be obtained using $\mu_\alpha = 0.107$. The activation volume V_α^*, however, had to be adopted to describe the data well. A value of 2.78 nm³ was needed, close to the value as determined for the Eyring flow rule. The rest of the parameters were equal to Table 4. With this parameter set, though, the tensile yield stresses were overpredicted. In order to get a similar result as shown in Figure 3b, the thermodynamic state parameter had to be decreased to $S_{a,\,\alpha} = 4.3$ for tensile tests.

5 | DISCUSSION

In an engineering approach, a description of the yield stress is often sufficient. Then, a pressure-dependent Ree-Eyring flow rule can be applied. Yet, for capturing more complex three-dimensional stress states, as it occurs in a polymer component during service life with variations along the product including both tensile and compressive stresses, employing the full EGP model is more appropriate. Furthermore, if a product is under long-term effects, for example, creep or fatigue, different material elements will be at different, changing strain and stress levels. Then, the use of a constitutive model that can describe the stress/strain behavior over large strains becomes necessary. Consequently, a yield criterion does not suffice.

5.1 | Pressure dependence

Uniaxial compression tests are an excellent tool to determine directly the true stress–strain behavior up to large strains, since homogeneous deformation can be obtained beyond the yield stress.[14,35] Of course, pressure-dependence can not be detected if tests under a single loading geometry are performed. In fact, for different values of μ_α, various parameter sets were generated by fitting the compression data. Most EGP model parameters did not need to change (see Table 4), except for the activation volume V_α^*, to describe the experimental compression data equally well (see Figure 6a). With these parameter sets, subsequently the tensile behavior was simulated. As can be seen in Figure 7, a value for the pressure-dependence parameter of $\mu_\alpha = 0.15$ gave the
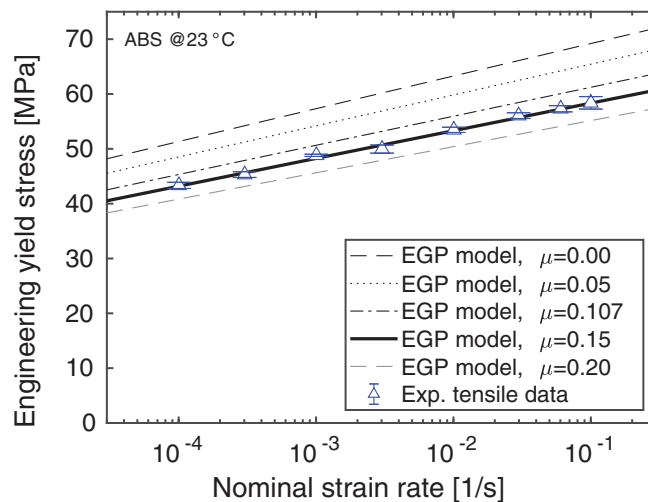

FIGURE 7 Engineering yield stresses as a function of decimal logarithmic strain rate in uniaxial tension. Symbols are experimental data, lines are model predictions [Color figure can be viewed at wileyonlinelibrary.com]

best agreement with the experimental data. The rest of the parameter sets over- or underpredicts the data. This may be corrected for by a change in the thermodynamic state parameter $S_{a,\,\alpha}$, which may be justified as different sample geometries and machining operations may effect sample age.[35,65] However, $\mu_\alpha = 0.15$ also gave the best slope to describe the tensile $\sigma_y - \log(\dot{\varepsilon})$ curves. Logically, strain-rate dependence worsened as values for μ_α were further away from the ideal value. Using various parameter sets to determine pressure-dependence was also applied by Van Breemen et al.[68] They combined, though, uniaxial compression data with indentation tests.

5.2 | True versus nominal strain rate

As mentioned in Subsection 2.3, both tensile and compression tests were executed with nominal strain rates. Generally, though, uniaxial compression tests are operated with a constant true strain rate.[16,22,35] By using nominal strain rates, the true strain rate accelerates in compression, while it decelerates in tension tests. This, of course, causes differences in the experimental results. However, using a constant cross-head speed during experiments is, understandably, more straightforward and easy to implement.

Figure 8 demonstrates, numerically, the differences between applying a constant true strain rate ($\dot{\varepsilon} = 10^{-3}$ s⁻¹) and a nominal one ($\dot{\varepsilon}_0 = 10^{-3}$ s⁻¹). There is hardly any influence up to the upper yield stress and well within experimental error. This is also the case for a completely rejuvenated sample, that is, $S_a = 0$. On the other hand, it

does start to affect from the yield stress on, resulting in higher predictions of the lower yield stress and strain hardening for a nominal strain rate. Furthermore, as can be seen for the curves with $G_r = 0$, that is, no strain hardening, the nominal strain rate curve already intrinsically shows some strain hardening. This makes it more difficult to determine the strain hardening parameter G_r, causing the need for iteration steps by trial-and-error. Another clear disadvantage, also as a result of an accelerating true strain rate, is that the nominal strain rate compression tests are more prone to viscous heating. Moreover, as was seen in the present study, viscous heating will be more difficult to detect.
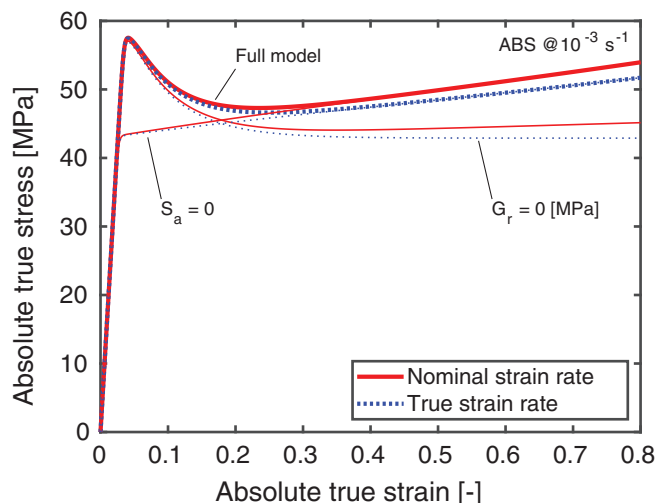

FIGURE 8 Numerical absolute true stress/strain curves at nominal or true strain rates. Model parameters as given in Table 4 [Color figure can be viewed at wileyonlinelibrary.com]

TABLE 3 Eyring model parameters for PMMA material

x	μ_x [−]	V_x^* [nm³]	ΔU_x [kJ mol⁻¹]	$\dot{\gamma}_{0,x}^{comp}$ [s⁻¹]	$\dot{\gamma}_{0,x}^{tens}$ [s⁻¹]
α	0.238	3.80	399	$6.73 \cdot 10^{49}$	$1.23 \cdot 10^{50}$
α'	0.428	2.28	103	$5.81 \cdot 10^{13}$	$2.68 \cdot 10^{13}$
β	0	1.09	103	$8.32 \cdot 10^{16}$	—

6 | CONCLUSIONS

A commercial grade ABS copolymer (Magnum™ 8434) has been mechanically characterized over a range of strain rates, both in uniaxial tensile and compression tests. By measuring in two different loading geometries, the influence of the hydrostatic pressure-dependence on the deformation behavior of the material can be established. This is an important aspect, since most polymer components undergo a complex stress state in service life, with both tensile and compressive stresses. Hence, a quantitative prediction of the material's behavior in both tension and compression is a significant aspect to correctly and safely design a polymer product.

Various methodologies to determine hydrostatic pressure-dependence of a polymer material have been revised. Among others, the direct measurement of tensile data under superimposed hydrostatic pressure. This is, however, a rather complex procedure for which special equipment is needed.[24,27,28] An alternative method to determine pressure-dependence has been presented. It is based on the observation that pressure-dependence manifests itself due to the differences in the hydrostatic part of the stress state under different loading geometries.[8,25] It takes the distinct strain-rate dependence for tension and compression into account, i.e. the slopes of the $\sigma_y - \log(\dot{\varepsilon})$ curves. Results from the present study showed it to be an effective technique.

Results for the ABS material showed thermorheological simple behavior. A single molecular process, represented by the α-relaxation mechanism, was sufficient to capture excellently the deformation behavior over the measured strain-rate range. The experimental results in compression manifested viscous heating at the two highest strain rates. A pressure-dependence parameter $\mu_\alpha = 0.15$ gives the best results to describe the experimental data in tension and compression simultaneously with a single set of model parameters.

The methodology using the different strain-rate dependence in distinct loading geometries to determine pressure-dependence was also successfully applied on a material with thermorheological complex behavior. The classical data of Bauwens-Crowet[41] for a commercial

TABLE 4 EGP model parameters for ABS magnum™ 8434 material

G_r [MPa]	κ [MPa]	$G_{\alpha,1}$ [MPa]	$\eta_{0,\alpha,1,ref}$ [MPa s]	$G_{\alpha,2}$ [MPa]	$\eta_{0,\alpha,2,ref}$ [MPa s]	ΔU_α [a] [kJ mol⁻¹]
4	1860	620	$3 \cdot 10^9$	100	$3 \cdot 10^{-2}$	257
T_{ref} [K]	V_α^* [nm³]	μ_α [−]	$S_{0,\alpha}$ [−]	$r_{0,\alpha}$ [−]	$r_{1,\alpha}$ [−]	$r_{2,\alpha}$ [−]
296	2.86	0.15	5.4	0.99	50	− 7

[a]Data taken from Truss & Chadwick.[5]

grade Poly(Methyl MethAcrylate) Perspex ICI (PMMA) measured in compression and tension over a wide range of strain-rates and temperatures could be remarkably well described. It was illustrated that every molecular relaxation process has its own pressure-dependence associated with it.

Although the yield criterion (based on an Eyring-type pressure-modified rate equation) is able to outstandingly describe the yield stresses of ABS, it is unable to describe the more complex three-dimensional stress state that appear in a polymer component in service life. The fully three-dimensional visco-elasto-plastic constitutive Eindhoven Glassy Polymer (EGP) model, on the other hand, is able to quantitatively represent the large-strain deformation behavior of this material. Therefore, this model is also more appropriate to simulate a polymer component's long-term behavior as it occurs under creep circumstances or due to fatigue, as was manifested by previous research.[17,22]

A methodology has been presented to mechanically characterize a polymer material and determine model parameters for both an engineering approach (a yield criterion) and a full 3D constitutive model that includes the resolution of the material's pressure-dependence. Such measurements are a first step to conceive an adequate engineering design framework able to deal with multi-axial stress states. It will be suitable to determine the large-strain mechanical response in Finite Element simulations for the development of polymer components.

ACKNOWLEDGMENTS

AUTHOR CONTRIBUTIONS

Wilco M.H. Verbeeten: Conceptualization (lead); funding acquisition (equal); investigation (equal); methodology (lead); project administration (equal); validation (equal); visualization (lead); writing – original draft (lead); writing – review & editing (equal). **Miguel Sánchez-Soto**: Conceptualization (supporting); investigation (equal); methodology (supporting); project administration (equal); validation (equal); visualization (supporting); writing – review and editing (equal). **Maria Lluisa Maspoch**: Conceptualization (supporting); investigation (equal); methodology (supporting); project administration (lead); validation (equal); visualization (supporting); writing – review and editing (equal).

DATA AVAILABILITY STATEMENT
Data available on request from the authors.

ORCID
Wilco M. H. Verbeeten https://orcid.org/0000-0001-7026-1642
Miguel Sánchez-Soto https://orcid.org/0000-0002-0023-5059
Maria Lluisa Maspoch https://orcid.org/0000-0002-4813-6412

REFERENCES
[1] Ceresana, *Market Study: Engineering Plastics*, 4th ed., Ceresana, Constance, Germany **2021**.
[2] W.-S. Lee, H.-L. Lin, *The Strain Rate Dependence of Deformation and Fracture Behaviour of ABS*, Elsevier Ltd, Oxford, United Kingdom **2003**, p. 231.
[3] P. Zítek, S. Myšík, J. Zelinger, *Angew Makromol Chem* **1969**, *6*, 116.
[4] A. Casale, O. Salvatore, G. Pizzigoni, *Polym Eng Sci* **1975**, *15*, 286.
[5] R. Truss, G. Chadwick, *J Mater Sci* **1976**, *11*, 111.
[6] C. Bucknall, *Toughened Plastics, Materials Science Series*, Applied Science Publishers Ltd, London **1977**.
[7] A. Donald, E. Kramer, *J Mater Sci* **1982**, *17*, 1765.
[8] C. Chen, J. Sauer, *J Appl Polym Sci* **1990**, *40*, 503.
[9] C. Bernal, P. Frontini, M. Sforza, M. Bibbó, *J Appl Polym Sci* **1995**, *58*, 1.
[10] J. Dear, J. Graham, P. Brown, *Polymer* **1998**, *39*, 2349.
[11] X. Xu, R. Wang, Z. Tan, H. Yang, M. Zhang, H. Zhang, *Eur Polym J* **2005**, *41*, 1919.
[12] Z. Tan, X. Xu, S. Sun, C. Zhou, Y. Ao, H. Zhang, Y. Han, *Polym Eng Sci* **2006**, *46*, 1476.
[13] X. Xu, X. Xu, *Polym Eng Sci* **2011**, *51*, 902.
[14] M. Boyce, E. Arruda, R. Jayachandran, *Polym Eng Sci* **1994**, *34*, 716.
[15] P. Wu, E. van der Giessen, *Int J Plast* **1995**, *11*, 211.
[16] H. van Melick, L. Govaert, H. Meijer, *Polymer* **2003**, *44*, 3579.
[17] E. Klompen, T. Engels, L. van Breemen, P. Schreurs, L. Govaert, H. Meijer, *Macromolecules* **2005**, *38*, 7009.
[18] L. Govaert, T. Engels, S. Söntjens, T. Smit, *Time-Dependent Failure in Load-Bearing Polymers. A Potential Hazard in Structural Applications of Polylactides*, Nova Science Publishers, Inc., New York **2009**, pp. 21–39.
[19] R. Quinson, J. Perez, M. Rink, A. Pavan, *J Mater Sci* **1997**, *32*, 1371.
[20] H. Niklas, H. Kausch von Schmeling, *Kunststoffe* **1963**, *53*, 886.
[21] I. Narisawa, M. Ishikawa, H. Ogawa, *J Polym Sci Polym Phys Ed* **1978**, *16*, 1459.
[22] R. Janssen, D. de Kanter, L. Govaert, H. Meijer, *Macromolecules* **2008**, *41*, 2520.
[23] M. Kanters, K. Remerie, L. Govaert, *Polym Eng Sci* **2016**, *56*, 676.
[24] G. Biglione, E. Baer, S. Radcliffe, *Proceedings of the Second International Conference on Fracture*, Paper 44, Chapman and Hall, London, United Kingdom **1969**, p. 503.
[25] G. Dean, L. Wright, *Polym Test* **2003**, *22*, 625.

[26] H. Louche, F. Piette-Coudol, R. Arrieux, J. Issartel, *Int J Impact Eng* **2009**, *36*, 847.

[27] W. Vroom, R. Westover, *SPE J* **1969**, *25*, 58.

[28] J. Sauer, *Polym Eng Sci* **1977**, *17*, 150.

[29] L. Govaert, H. Schellens, H. Thomassen, R. Smit, L. Terzoli, T. Peijs, *Composites A* **2001**, *32*, 1697.

[30] I. Ward, *J Mater Sci* **1971**, *6*, 1397.

[31] C. Bauwens-Crowet, J.-C. Bauwens, G. Homès, *J Mater Sci* **1972**, *7*, 176.

[32] R. Duckett, B. Goswami, L. Smith, I. Ward, A. Zihlif, *Br Polym J* **1978**, *10*, 11.

[33] H. Visser, T. Bor, M. Wolters, T. Engels, L. Govaert, *Macromol Mater Eng* **2010**, *295*, 637.

[34] C. Buckley, P. Dooling, J. Harding, C. Ruiz, *J Mech Phys Solids* **2004**, *52*, 2355.

[35] E. Klompen, T. Engels, L. Govaert, H. Meijer, *Macromolecules* **2005**, *38*, 6997.

[36] R. Smit, W. Brekelmans, H. Meijer, *Comput Methods Appl Mech Eng* **1998**, *155*, 181.

[37] R. Smit, W. Brekelmans, H. Meijer, *J Mech Phys Solids* **1999**, *47*, 201.

[38] R. Smit, W. Brekelmans, H. Meijer, *J Mater Sci* **2000**, *35*, 2869.

[39] R. J. M. Smit, W. A. M. Brekelmans, H. E. H. Meijer, *Journal of Materials Science* **2000**, *35*, 2881. http://dx.doi.org/10.1023/a:1004715707138.

[40] W.-S. Lee, H.-C. Shen, *Mater Sci Technol* **2004**, *20*, 8.

[41] C. Bauwens-Crowet, *J Mater Sci* **1973**, *8*, 968.

[42] L. Govaert, P. Timmermans, W. Brekelmans, *J Eng Mater Technol* **2000**, *122*, 177.

[43] J. Roetling, *Polymer* **1965**, *6*, 311.

[44] C. Bauwens-Crowet, J. Bauwens, G. Homès, *J Polym Sci Part A-2 Polym Phys* **1969**, *7*, 735.

[45] J. Sauer, D. Mears, K. Pae, *Eur Polym J* **1970**, *6*, 1015.

[46] T. Engels, S. Söntjens, T. Smit, L. Govaert, *J Mater Sci Mater Med* **2010**, *21*, 89.

[47] L. van Breemen, T. Engels, E. Klompen, D. Senden, L. Govaert, *J Polym Sci B Polym Phys* **2012**, *50*, 1757.

[48] M. Wendlandt, T. Tervoort, U. Suter, *Polymer* **2005**, *46*, 11786.

[49] R. Haward, G. Thackray, *Proc Royal Soc London Ser A Math Phys Eng Sci* **1968**, *302*, 453.

[50] T. Ree, H. Eyring, *J Appl Phys* **1955**, *26*, 793.

[51] J. De Deus, G. Souza, W. Corradini, T. Atvars, L. Akcelrud, *Macromolecules* **2004**, *37*, 6938.

[52] T. Tervoort, E. Klompen, L. Govaert, *J Rheol* **1996**, *40*, 779.

[53] L. van Breemen, E. Klompen, L. Govaert, H. Meijer, *J Mech Phys Solids* **2011**, *59*, 2191.

[54] H. Pugh, E. Chandler, L. Holliday, J. Mann, *Polym Eng Sci* **1971**, *11*, 463.

[55] J. Bauwens, *J Polym Sci Part A-2 Polym Phys* **1970**, *8*, 893.

[56] P. Bowden, J. Jukes, *J Mater Sci* **1972**, *7*, 52.

[57] R. Bubeck, S. Bales, H.-D. Lee, *Polym Eng Sci* **1984**, *24*, 1142.

[58] L. Govaert, T. Engels, E. Klompen, G. Peters, H. Meijer, *Int Polym Process* **2005**, *20*, 170.

[59] W. Verbeeten, M. Kanters, T. Engels, L. Govaert, *Polym Int* **2015**, *64*, 1527.

[60] C. Bauwens-Crowet, J.-C. Bauwens, *Polymer* **1982**, *23*, 1599.

[61] E. Arruda, M. Boyce, R. Jayachandran, *Mech Mater* **1995**, *19*, 193.

[62] M. Wyzgoski, *J Appl Polym Sci* **1980**, *25*, 1443.

[63] J. Martins, T. Klohn, O. Bianchi, R. Fiorio, E. Freire, *Polym Bull* **2010**, *64*, 497.

[64] A. Díez-Pascual, D. Gascón, *ACS Appl Mater Interfaces* **2013**, *5*, 12107.

[65] T. Engels, L. van Breemen, L. Govaert, H. Meijer, *Macromol Mater Eng* **2009**, *294*, 829.

[66] E. Klompen, L. Govaert, *Mech Time-Dep Mater* **1999**, *3*, 49.

[67] E. Thompson, *J Polym Sci Part A-2 Polym Phys* **1968**, *6*, 433.

[68] L. van Breemen, T. Engels, C. Pelletier, L. Govaert, J. den Toonder, *Philos Mag* **2009**, *89*, 677.

SUPPORTING INFORMATION

Additional supporting information may be found in the online version of the article at the publisher's website.